Shot noise measurements in graphene

Danneau, R.; Wu, F.; Craciun, M.F.; Russo, S.; Tomi, M.Y.; Salmilehto, J.; Morpurgo, Alberto; Hakonen, P.J.

Solid State Communications 149 (2009) 1050–1055

Contents lists available at ScienceDirect

Solid State Communications

journal homepage: www.elsevier.com/locate/ssc

Shot noise measurements in graphene

R. Danneau [a,1], F. Wu [a], M.F. Craciun [b,2], S. Russo [b,2], M.Y. Tomi [a], J. Salmilehto [a], A.F. Morpurgo [c], P.J. Hakonen [a,*]

[a] Low Temperature Laboratory, Helsinki University of Technology, Espoo, Finland
[b] Kavli Institute of Nanoscience, Delft University of Technology, Delft, The Netherlands
[c] DPMC and GAP, University of Geneva, quai Ernest-Ansertmet 24, CH1211 Geneva, Switzerland

ARTICLE INFO

Article history:
Received 30 November 2008
Accepted 5 February 2009 by Guest Editors
Available online 20 March 2009

PACS:
72.80.Rj
73.23.Ad
72.70.+m
73.50.Td

Keywords:
A. Nanostructures
D. Electronic transport
D. Noise

ABSTRACT

We have investigated shot noise at microwave frequencies in wide-aspect-ratio graphene sheets in the temperature range of 4.2–30 K. We find that for our short ($L < 300$ nm) graphene samples with width over length ratio $W/L > 3$, the Fano factor $\mathfrak{F}$ reaches a maximum $\mathfrak{F} \sim 1/3$ at the Dirac point and that it decreases substantially with increasing charge density. Our results agree with the theoretical prediction that electrical transport at the Dirac point is governed by evanescent electronic states.

1. Introduction

Single layer graphite, graphene, is a unique semiconductor material [1]. It is gapless, as its cone-like conduction and valence bands touch at two inequivalent Dirac points, K and K′, where the density of states vanishes. The conductivity at the Dirac point, however, remains finite. It has been theoretically shown that in perfect graphene at the Dirac point, the conduction occurs only via evanescent waves, i.e. via tunneling between the leads [2,3]. This has interesting consequences on the conductivity and on the shot noise, both of which display universal behavior in the limit of wide-aspect-ratio sheets.

In this article, we discuss experimental results on shot noise in short and wide graphene strips [4]. Using a cryogenic, low-noise amplification set-up, we measure shot noise as a function of the gate voltage in two-terminal field-effect graphene devices. The results are successfully compared with the theoretical values derived by solving the Dirac equation [2,3]. Even though the shot noise at the Dirac point is equivalent to that of a regular diffusive conductor, clear distinction in the noise behavior can be found in the gate dependence. Therefore, our results on short, less than 300 nm long samples with large width-over-length ratio $W/L > 3$ provide support for the theoretical "pseudodiffusive" transport picture of ballistic graphene. We also show and discuss how disorder affects the conductivity and the shot noise in our longer samples.

2. Theoretical background

The conductance of a single transmission channel can be written as $G = g\frac{e^2}{h}\tau$, where g is the degeneracy (spin and valley) of the system and τ the electron transmission probability. When the system is biased, shot noise appears due to discreteness of charge [5] and these current fluctuations for a single channel are given by $\langle(\delta I)^2\rangle = 2e\langle I\rangle(1-\tau)$. The total noise power spectrum for a multichannel conductor is then obtained by summing over all N transmission eigenchannels:

$$S_I = \frac{2e^3|V|}{h}\sum_{n=0}^{N-1}\tau_n(1-\tau_n). \quad (1)$$

In the limit of low transparency $\tau_n \ll 1$,

$$S_I \cong S_{Poisson} = \frac{2e^3|V|}{h}\sum_{n=0}^{N-1}\tau_n = 2e\langle I\rangle, \quad (2)$$

* Corresponding author.
E-mail address: pjh@boojum.hut.fi (P.J. Hakonen).

[1] Present address: Institut für Nanotechnologie, Forschungszentrum Karlsruhe and Physikalisches Institut, Universität Karlsruhe, Karlsruhe Institut of Technology, Germany.

[2] Present address: Department of Applied Physics, University of Tokyo, Japan.

0038-1098/$ – see front matter © 2009 Elsevier Ltd. All rights reserved.
doi:10.1016/j.ssc.2009.02.046

defining a Poissonian noise induced by independent and random electrons like in tunnel junctions [5]. The regular way to quantify shot noise is to use the Fano factor $\mathfrak{F}$ which is the ratio between the measured shot noise and the Poissonian noise:

$$\mathfrak{F} = \frac{S_I}{S_{Poisson}} = \frac{S_I}{2e\langle I\rangle} = \frac{\sum_{n=0}^{N-1}\tau_n(1-\tau_n)}{\sum_{n=0}^{N-1}\tau_n}. \quad (3)$$

Then, for a Poissonian process $\mathfrak{F} = 1$ at small transparency ($\tau_n \to 0$), while $\mathfrak{F} = 0$ in the ballistic regime (i.e. when $\tau_n \to 1$) and $\mathfrak{F} = 1/3$ in the case of a diffusive system.

In graphene, it has been theoretically concluded that transport at the Dirac point occurs via electronic evanescent waves [2,3]. Tworzydło et al. used heavily-doped graphene leads and the wave function matching method to directly solve the Dirac equation in perfect graphene with length L and width W [3]. They found that for armchair edges, the quantization condition of the transverse wave vector is defined by $k_{y,n} = \frac{(n+\alpha)}{W}\pi$ where $\alpha = 0$ or $\frac{1}{3}$ for metallic and semiconducting armchair edges, respectively. At the Dirac point, the transmission coefficients are given by:

$$\tau_n^{Dirac} = \frac{1}{\cosh^2(\pi(n+\alpha)\frac{L}{W})}. \quad (4)$$

Consequently, graphene has a similar bimodal distribution of transmission eigenvalues at the Dirac point as there is in diffusive systems [6,7]. In the limit of $W/L \to \infty$, the mode spacing becoming small and one can replace the sum over the channels by an integral over the transverse wave vector component k_y to obtain the conductivity and the Fano factor for a sheet with metallic armchair edge:

$$\sigma_{Dirac} = G_{Dirac}\frac{L}{W} = \frac{4e^2}{h}\frac{L}{W}\int_0^\infty \frac{dk_y}{\cosh^2(k_yL)} = \frac{4e^2}{\pi h}, \quad (5)$$

$$\mathfrak{F}_{Dirac} = \frac{\sum_{n=0}^{N-1}\tau_n^{Dirac}(1-\tau_n^{Dirac})}{\sum_{n=0}^{N-1}\tau_n^{Dirac}} = \frac{1}{3}. \quad (6)$$

At the Dirac point, the conductivity is at minimum ($\sigma_{Dirac} = \frac{4e^2}{\pi h}$) and the Fano factor is at maximum ($\mathfrak{F}_{Dirac} = \frac{1}{3}$) [3]. Equivalent results have been obtained with more realistic contact conditions as well [8]. However, both conductivity and Fano factor are no longer at minimum and maximum, respectively, when the transport becomes incoherent [9]. Moreover, in large samples the minimum conductivity has been measured to be around $\sigma_{Dirac} = \frac{4e^2}{h}$ [1,10,11], which points towards the presence of disorder [12]. By tuning the carrier density, the Fermi level is moved away from the Dirac point where the density of states is no longer zero. At large density the number of conducting channels increases, the evanescent states are then accompanied by propagating states, and the conductivity rises while the Fano factor decreases [3].

Let us note that the result $F = 1/3$ seems to be a rather robust result in graphene, and it resurfaces in several different contexts. The Fano factor for a bilayer system has been predicted to be $\frac{1}{3}$ as well [13] or $1 - \frac{2}{\pi}$ [14], i.e. very close to $\frac{1}{3}$. Moreover, even if there are pn-junctions present in the graphene sample, the Fano factor is expected to be very close to $\frac{1}{3}$ [15], though it will vary depending on the Landau level filling factors in a magnetic field [16].

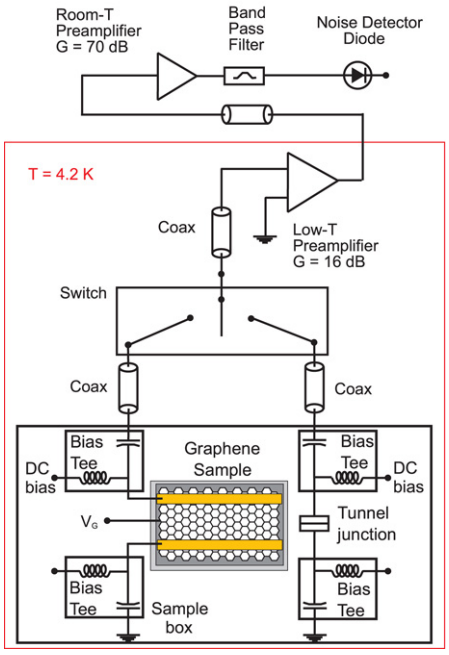

Fig. 1. (Color online) Experimental set-up for detecting shot noise at $T = 4.2$–30 K.

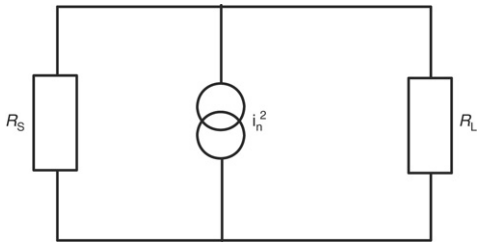

Fig. 2. Schematic of the equivalent circuit of our measurement: R_S and Z_0 represent the resistance of the sample and the cold preamplifier respectively, i_n^2 represents the full noise generated by the circuit.

3. Experimental set-up and shot noise measurement technique

We employ microwave frequencies to implement a sensitive noise measurement scheme based on lock-in detection of modulated current fluctuations (see Refs. [17,18,4] for details). The bias current I_{DC} is modulated using a sine-wave modulation, $I = I_{DC} + \delta I\sin(\omega t)$ where $I_{DC} \gg \delta I$, for the lock-in detection of noise. Alternatively, shot noise can also be detected without current modulation using a DC scheme. We employ the shot noise generated by a tunnel junction with Poissonian noise ($\mathfrak{F} = 1$) to calibrate the measurement sensitivity. A detailed discussion on our measurement setup (Fig. 1), as well as sample preparation, can be found in Ref. [19].

By using the equivalent electrical model shown in Fig. 2, we can calculate the coupled noise power of the current fluctuations to the first-stage cold amplifier. The noise generator ${i_n}^2$ is a sum of the generators of the amplifier with resistance $R_L = 50\ \Omega$ and the sample with resistance R_S

$$\begin{aligned} {i_n}^2 &= \frac{4k_BT_N}{R_L} + S_I \\ &= \frac{4k_BT_N}{R_L} + \frac{4k_BT}{R_S}\left[1 - \mathfrak{F} + \mathfrak{F}\cdot\frac{eIR_S}{2k_BT}\coth\left(\frac{eV}{2k_BT}\right)\right] \end{aligned} \quad (7)$$

which is dependent on the current I and voltage V across the sample, and where T_N denotes the noise temperature of the amplifier, T is the bath temperature of the reservoir, and $\mathfrak{F}$

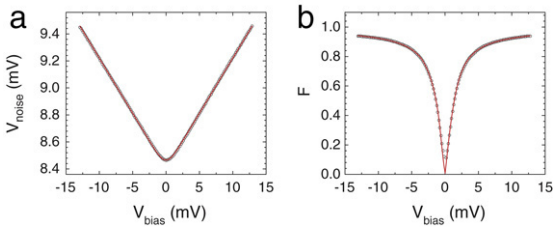

Fig. 3. (Color online) Typical tunnel junction noise measurement data: (a) as used for noise power calibration, and (b) for $F(V_{bias})$ investigations (b). The red curves are fits based on the Khlus formula at $T = 4.4$ K: Eq. (7) in (a) and Eq. (10) in (b).

indicates the (bias-dependent) Fano factor. The first term on the right hand side describes the noise from the amplifier, while the second term S_I is the sum of thermal and shot noise coming from the sample that we want to measure, which was originally introduced by Khlus [20] to describe the cross-over from thermal to shot noise; its value starts from $\frac{4k_BT}{R_S}$ at zero bias and approaches $\mathfrak{F} \cdot 2eI$ at $eV \gg k_BT$. The spectral power coupled to the amplifier becomes $S_P = {i_n}^2 \cdot (\frac{R_S}{R_S+R_L})^2 R_L$ according to the circuit model, and the measured noise power

$$P = S_P \cdot g_A \cdot BW = {i_n}^2 \cdot \left(\frac{R_S}{R_S + R_L}\right)^2 R_L \cdot g_A \cdot BW, \tag{8}$$

where g_A and BW denote the gain and bandwidth of the amplifier chain, respectively.

In practical measurements, g_A and BW can be calibrated straightforwardly by a tunnel junction with $\mathfrak{F} = 1$, but T_N is not an easily-measurable parameter. Therefore, we define an average Fano factor using the excess noise

$$F = (S_I(I) - S_I(0))/(2eI) \tag{9}$$

which can be directly deduced from the measured noise power vs. current. Notice that $F \to \mathfrak{F}$ at $eV \gg k_BT$, while $F \to 0$ at small bias due to thermal noise averaging. For nonlinear samples in which R_S is dependent on the bias voltage, we need to make nonlinearity corrections to convert measured S_P into S_I [18,19], but for graphene samples with nearly constant $R_S(V)$, we can directly deduce the relation between F and $\mathfrak{F}$ from Eq. (7), which yields

$$F = \mathfrak{F} \cdot \left[\left(\frac{eV}{2k_BT}\coth\frac{eV}{2k_BT} - 1\right) \Big/ \frac{eV}{2k_BT}\right]. \tag{10}$$

By expanding Eq. (10) to 2nd order in V at low bias, we can relate the Fano factor $\mathfrak{F}$ to the linear slope of $F(V_{bias})$. This method requires accurate knowledge of the temperature and, unfortunately, it becomes unreliable in the presence of reservoir heating.

Fig. 3 illustrates the high resolution of our experimental calibration on a typical tunnel junction sample with resistance $R_T = 8\ k\Omega$. In Fig. 3(a) the measured noise power is fitted with Eqs. (7) and (8) using $\mathfrak{F} = 1$; this yields a calibration that is based mostly on the high bias slope of the data. Fig. 3(b), on the other hand, displays the calculated average Fano factor F vs. V_{bias}, together with the expectation from Eq. (10); the intercomparison of the two is sensitive to deviations from constant T (or constant $\mathfrak{F}$) at low bias. The perfect agreement in Fig. 3(a) and (b) indicates that our calibration is trustworthy and that there is no substantial reservoir heating affecting our calibration.

4. Results on shot noise

Here, we discuss results of four samples which are listed in Table 1: the set represents our submicron long samples with the largest aspect ratio W/L. According to the theory, results in such samples should be universal, which allows for the most pertinent comparison between experiment and theory.

Table 1
Characteristics of our four samples. W/L is the width over length ratio. V_D defines the position of the Dirac point in gate voltage. These points were extrapolated from the minimum conductivity at $\frac{4e^2}{\pi h}$ for samples II and III. See text for more details.

Sample I	Sample II	Sample III	Sample IV
$\frac{W}{L} = 24$	$\frac{W}{L} = 10$	$\frac{W}{L} = 3$	$\frac{W}{L} = 4.2$
$L = 200$ nm	$L = 200$ nm	$L = 300$ nm	$L = 950$ nm
$V_D = 19.5$ V	$V_D = 145$ V	$V_D = 100$ V	$V_D = 28$ V

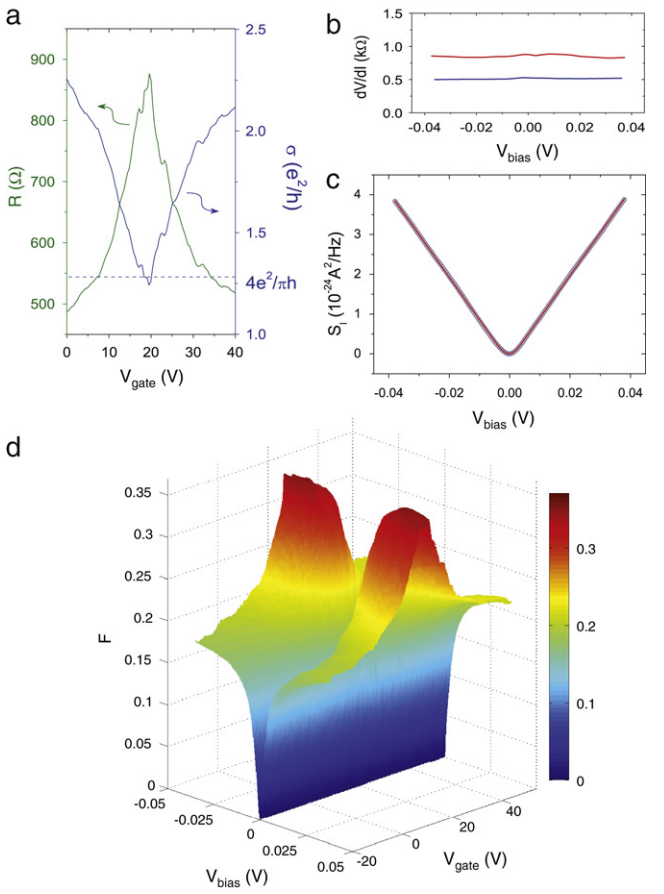

Fig. 4. (Color online) DC transport and shot noise measurements on sample A: (a) Resistance R (left axis) and conductivity σ (right axis) as a function of V_{gate}. (b) Differential resistance dV/dI versus bias voltage V_{bias} at the Dirac point (red curve) and at high density (blue curve). (c) Current noise per unit bandwidth S_I as a function of bias at the Dirac point, at $T = 8.5$ K, fitted (red curve) using Khlus formula ($\mathfrak{F} = 0.318$). (d) Mapping of the average Fano factor F as a function of gate voltage V_{gate} and bias voltage V_{bias} at $T = 8.5$ K.

Sample I has an aspect ratio of $W/L = 24$. Fig. 4(a) displays the resistance and conductivity of sample I as functions of the gate voltage (i.e. charge carrier density). All of our graphene samples show a maximum resistance in positive gate voltage V_{gate} values. This means that our samples are non-intentionally p-doped, probably due to oxygen gas adsorption [21]. We observe a maximum resistance and a minimum conductivity of around $\frac{4e^2}{\pi h}$ at the Dirac point. For sample I, we obtain a minimum conductivity which is the one expected for large aspect ratio graphene strips [3] and observed experimentally in recent experiments [22]. In these samples the resistance was nearly independent of the bias voltage V_{bias}, regardless of whether the measurement was taken at, or far away from, the Dirac point (see Figs. 4(b) and 7(b)).

Fig. 4(c) displays the current noise per unit bandwidth as a function of V_{bias} measured at the Dirac point at $T = 8.5$ K in sample

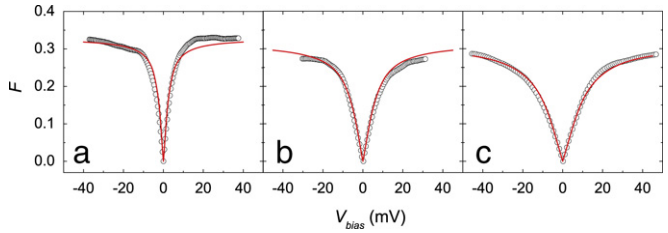

Fig. 5. Average Fano factor F versus source drain bias V_{bias} at charge neutrality point (Dirac point) measured at three different temperatures: (a) $T = 8.5$ K, (b) $T = 19.6$ K and (c) $T = 32$ K. The red solid curve in each frame displays $F(V_{bias})$ calculated from Eq. (10) with $\mathfrak{F} = 0.33$, 0.32, and 0.32 at the respective temperatures. Notice that in frame (a) the value of F measured at low bias is a bit smaller than the theoretical prediction.

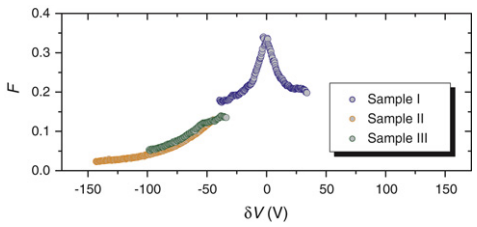

Fig. 6. (Color online) Average Fano factor F extracted at V_{bias} = 40 mV for samples I-III, all having $W/L \geq 3$, as a function of $\delta V = V_{gate} - V_{Dirac}$, where V_{Dirac} is the gate voltage value to reach the Dirac point.

I. By using the Khlus formula, Eq. (7), we obtain for the Fano factor $\mathfrak{F} = 0.318$ [20]. We have also used excess noise (cf. Eq. (9)) to extract the average Fano factor F [17,18,4], which yields $F = 0.338$ at the Dirac point (at $V_{bias} = 40$ mV).

Our measurements seem to confirm that transport at the Dirac point occurs via evanescent waves [2,3]. The two extracted Fano factors $\mathfrak{F}$ and F as well as the minimum conductivity are very close to the expected theoretical values of $\frac{1}{3}$ and $\frac{4e^2}{\pi h}$, respectively, at the Dirac point for a perfect graphene strip with large W/L [3]. Note that this measured Fano factor at the Dirac coincides also with the expected result for a regular, diffusive mesoscopic system. In Ref. [3], the authors demonstrate that, in graphene, the Fano factor should decrease as the charge carrier density increases whereas no decrease with V_{gate} should take place for a common diffusive system.

Fig. 4(d) presents a scan of the average Fano factor F on the plane spanned by the bias voltage V_{bias} and by the gate voltage V_{gate}. A clear dependence of F on V_{gate} (i.e. the charge carrier density) is observed, with a clear drop (about a factor of 2) of the Fano factor at large carrier density. This gate dependence, in addition to the observation of the minimum conductivity at $\frac{4e^2}{\pi h}$ and a maximum Fano factor of $\frac{1}{3}$ at the Dirac point, all coincide with the expectations of the evanescent state theory [3]. We cannot, however, obtain a quantitative agreement of $F(V_{gate})$ and $\sigma(V_{gate})$ with the evanescent mode theory, because doping by the leads causes a modification of the gate coupling capacitance. Consequently, the gate voltage dependence becomes weaker than the calculated one in Ref. [3]. Comparing our data with a square lattice contact model in perfect graphene strips with large W/L [23], we find that the capacitance C_{gate} in our sample is smaller by a factor of ∼9 compared with the estimate from a simple parallel plate capacitor model (i.e. $C_{gate} \sim 12$ aF/μm^2 instead of 115 aF/μm^2).

In order to illustrate the temperature dependence of our data at the Dirac point, we present $F(V_{bias})$ of sample I at three different temperatures in Fig. 5. We notice that $\mathfrak{F}$ remains near 1/3 and is barely affected by temperature up to T = 30 K; the V_{bias} dependence of F, on the other hand, becomes much slower with voltage as given by Eq. (10). Since our shot noise results do not depend on temperature ($\mathfrak{F}$ = const. between 4 and 30 K) and with our contacts being highly transparent, the presence of inelastic scattering mechanism in the graphene sample, or at its contacts, can be ruled out. Note that if the contacts were bad, the Fano factor would grow toward the limit of two symmetrical tunneling barriers in series (i.e. $R_{T1} = R_{T2}$):

$$\mathfrak{F} = \frac{R_{T1}^2 + R_{T2}^2}{(R_{T1} + R_{T2})^2} \rightarrow \frac{1}{2}. \tag{11}$$

This is not the case for our samples in which the measured Fano factor has never exceeded $\frac{1}{3}$.

Although the Khlus formula with constant $\mathfrak{F}$ applies to our measured $S_I(V_{bias})$ data (see Figs. 4(c) and 7(c)), the fitting error increases at low bias when $eV \sim k_BT$ as the thermal noise becomes more and more dominant. To study the low bias noise behavior of our samples, it is more accurate to investigate the average Fano factor and to compare the theoretical expectation from Eq. (10) with the measured data using a constant $\mathfrak{F} \sim 1/3$; this comparison is done in Fig. 5(a–c) for temperatures $T = 8.5$, 19.6, and 32 K, respectively. The data on $F(V_{bias})$ fit well with Eq. (10) at T = 19.6 and 32 K, indicating that the Fano factor $\mathfrak{F}$ is independent of bias voltage. However, there is a small deviation from the theoretical curve at the lowest temperature ($T = 8.5$ K) in Fig. 5(a), which indicates that F at low bias might be smaller than at high bias. Similar behavior has been observed in a few of other graphene samples and, even more strongly, in multi-walled carbon nanotubes. We ascribe this phenomenon to Joule heating of the reservoirs, most likely the graphene below the metallic electrodes. Since the electron–phonon coupling strength is weak, the section of graphene sample underneath the contacts will be heated up to a higher temperature than the metallic lead, which is expected to be at the bath temperature T. Consequently, the calculated value of F will be smaller as we have to use higher reservoir temperature T_{eff} in Eq. (10). If we adopt a constant $\mathfrak{F} = 0.33$ along the whole bias range, one can fit an effective temperature of $T_{eff} = 10$ K in Fig. 5(a) at low bias.[4] This heating effect will become less important at large bias because the shot noise will eventually take over fully and, thus, the value of F saturates. Other mechanisms that can change the measured Fano factor include electron–electron interactions [24,5], incoherent scattering [9], and thermal gradients in the metallic lead due to heat diffusion [25]. However, the first two processes should lead to $\mathfrak{F} = 1/3$ as $V_{bias} \rightarrow 0$ and higher $\mathfrak{F}$ in the high bias regime (i.e. increased slope of $F(V_{bias})$ at intermediate V_{bias}). The third mechanism is possible, but we cannot distinguish it from the heating of the graphene reservoir.

In addition to sample I, we have measured three other samples II-IV all having $W/L \geq 3$. The average Fano factor F as a function of $\delta V = V_{gate} - V_{Dirac}$ is plotted in Fig. 6 for samples I, II and III. All samples were p-doped, the Dirac points being at positive gate voltages, but only for one of these three samples could we reach the Dirac point (sample I). The gate voltages corresponding to the Dirac point for the two other samples were estimated from their conductivity curves. Despite the high doping level of the samples, the Fano factor seems to behave universally and tends to zero at very high density. This indicates that graphene can behave as a ballistic conductor, contradicting some of the recent arguments [26]. Despite the probable presence of some disorder in our system, the transport regime can be considered to be ballistic on the length scale of our shortest samples.

4.1. Effect of disorder

Disorder can strongly influence electronic transport in mesoscopic conductors. Fano factor of $\frac{1}{3}$ has been predicted [6,7] and

[4] Assuming that the heat conductivity from the graphene reservoir to the metallic lead is governed by Wiedemann-Franz law and limited by the interfacial contact resistance R_C, we get an upper limit estimate for $R_C = 20\ \Omega$.

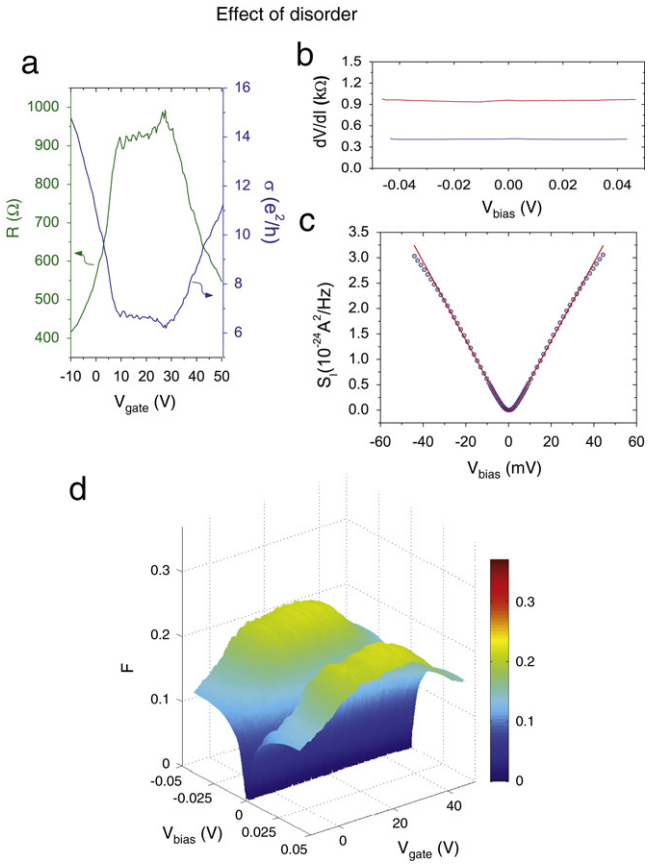

Fig. 7. (Color online) DC transport and shot noise measurements on sample IV: (a) Resistance R (left axis) and conductivity σ (right axis) as a function of gate voltage V_{gate}. (b) Differential resistance dV/dI versus bias voltage V_{bias} at the Dirac point (red curve) and at high density (blue curve). (c) Noise spectral density S_I as a function of bias voltage V_{bias} at the Dirac point, at $T = 12$ K, fitted (red curve) using Khlus formula ($\mathfrak{F} = 0.256$). (d) Mapping of the average Fano factor F as a function of gate voltage V_{gate} and bias voltage V_{bias} at $T = 12$ K.

experimentally verified in the case of diffusive systems [25]. Disordered multiwalled carbon nanotubes, on the other hand, have shown a broad spectrum of values [27]. Recent measurements in disordered graphene [28] have shown a gate-independent Fano factor and a value slightly above $\frac{1}{3}$, which could be due to bad graphene-contact interfaces or strong potential disorder [29]. Recent theories imply that disorder should enhance conductivity in graphene via impurity-induced resonant tunneling [30]. Such counterintuitive behavior can be understood as a consequence of the absence of intervalley scattering [31] and the chirality conservation [32]. It has also been shown that weak disorder may induce anomalously large conductance fluctuations at high carrier density [33]. By modeling smooth potential disorder, San Jose et al. have shown that near the Dirac point at length scales $\ll L, W$, disorder increases the minimum conductivity and lowers the Fano factor, down to 0.243 for one-dimensional disorder and to 0.295 for the two-dimensional case [34]. A regular, diffusive system should not display any gate dependence. Absence of gate dependence was demonstrated for long-range disorder in Ref. [29]. A gate-dependent Fano factor appears once the disorder strength is reduced.

Disorder effects start to play a role for our sample IV which has $W/L = 4.2$ and a large separation between the leads, approaching 1 μm. In Fig. 7(a), the resistance R and the conductivity σ are plotted against gate voltage V_{gate}. The resistance curve is not as peaked as it was in the short samples I–III, and in fact, the Dirac point seems to be truncated, probably due to the influence of disorder. Note that the graphene sheet is, again, p-doped. We also see that the minimum conductivity is no longer $\frac{4e^2}{\pi h}$ but much larger, which is also in agreement with the fact that disorder should increase the conductivity in graphene [30]. No bias dependence is observed in the differential resistance, as illustrated by Fig. 7(b).

In our noise measurements on sample IV, we observe a strong decrease of the Fano factor at the Dirac point compared with $\frac{1}{3}$ expected by the evanescent wave theory. Fig. 7(c) shows the noise spectral density measured at $T = 12$ K. Using Khlus formula, we extract a Fano factor at the Dirac point $\mathfrak{F} = 0.256$. The fit is not perfect at high bias probably due to electron–phonon coupling. We also note that the curve is slightly asymmetrical. The $F(V_{bias})$ analysis gives a smaller value of about 0.23 (see Fig. 7(d)). These values are in good agreement with the model which takes into account one dimensional smooth potential disorder [34]. In Fig. 7(d), we observe that the Fano factor is reduced by tuning the gate voltage V_{gate}, indicating that the disorder present in our sample appears to be smoother than in the samples of Ref. [28].

5. Conclusions

We studied transport and noise in submicron graphene strips with large W/L. At the Dirac point, we observed that for short samples ($L = 200$–300 nm) with $W/L > 3$ both minimum conductivity and Fano factor reach universal values of $\frac{4e^2}{\pi h}$ and $\frac{1}{3}$ respectively. At very large carrier density, the Fano factor tends to zero which is the value expected for a ballistic system. These findings are in accordance with the evanescent wave theory describing transport at the Dirac point in perfect graphene. When L is large enough, we see a significant reduction of the Fano factor at the Dirac point, reaching a value of 0.23, which is in good agreement with recent models taking into account smooth potential disorder like charge puddles [34].

Acknowledgments

We thank A. Castro Neto, Y. Hancock, A. Harju, T. Heikkilä, A. Kärkkäinen, M. Laakso, C. Lewenkopf, E. Mucciolo, M. Paalanen, P. Pasanen, E. Sonin, P. Virtanen and J. Wengler for fruitful discussions. This work was supported by the Academy of Finland, the EU CARDEQ contract FP6-IST-021285-2 and the NANOSYSTEMS project with Nokia Research Center.

References

[1] A.K. Geim, K.S. Novoselov, Nature Mat. 6 (2007) 183.
[2] M.I. Katsnelson, Eur. Phys. J. B 51 (2006) 157.
[3] J. Tworzydlo, B. Trauzettel, M. Titov, A. Rycerz, C.W.J. Beenakker, Phys. Rev. Lett. 96 (2006) 246802.
[4] R. Danneau, F. Wu, M.F. Craciun, S. Russo, M.Y. Tomi, J. Salmilehto, A.F. Morpurgo, P.J. Hakonen, Phys. Rev. Lett. 100 (2008) 196802.
[5] Y.M. Blanter, M. Büttiker, Phys. Rep. 336 (2000) 1.
[6] C.W.J. Beenakker, Phys. Rev. B 46 (1992) 1889.
[7] K. Nagaev, Phys. Lett. A 169 (1992) 103.
[8] H. Schomerus, Phys. Rev. B 76 (2007) 045433.
[9] E.B. Sonin, Phys. Rev. B 77 (2008) 233408.
[10] K.S. Novoselov, A.K. Geim, S.V. Morozov, D. Jiang, M.I. Katsnelson, I.V. Grigorieva, S.V. Dubonos, A.A. Firsov, Nature 438 (2005) 197.
[11] Y.-W. Tan, Y. Zhang, K. Bolotin, Y. Zhao, S. Adam, E.H. Whang, S. Das Sarma, H.L. Stormer, P. Kim, Phys. Rev. Lett. 99 (2007) 246803.
[12] J.H. Bardarson, J. Tworzydlo, P.W. Brouwer, C.W.J. Beenakker, Phys. Rev. Lett. 99 (2007) 106801.
[13] I. Snyman, C.W.J. Beenakker, Phys. Rev. B 75 (2007) 045322.
[14] M.I. Katsnelson, Eur. Phys. J. B 52 (2006) 151.
[15] V.V. Cheianov, V.I. Fal'ko, Phys. Rev. B 74 (2006) 041403(R).
[16] D.A. Abanin, L.S. Levitov, Science 317 (2007) 614.
[17] F. Wu, L. Roschier, T. Tsuneta, M. Palaanen, T.H. Wang, P.J. Hakonen, AIP Conf. Proc. 850 (2006) 1482.
[18] F. Wu, P. Queipo, A. Nasibulin, T. Tsuneta, T.H. Wang, E. Kauppinen, P.J. Hakonen, Phys. Rev. Lett. 99 (2007) 156803.

[19] R. Danneau, F. Wu, M.F. Craciun, S. Russo, M.Y. Tomi, J. Salmilehto, A.F. Morpurgo, P.J. Hakonen, J. Low Temp. Phys. 153 (2008) 374.
[20] V.A. Khlus, Zh. Ekps. Teor. Fiz. 93 (1987) 2179. [Sov. Phys. JETP 66, 1243].
[21] F. Schedin, A.K. Geim, S.V. Morozov, E.W. Hill, P. Blake, M.I. Katsnelson, K.S. Novoselov, Nature Mat. 6 (2007) 652.
[22] F. Miao, S. Wijeratne, Y. Zhang, U.C. Coskun, W. Bao, C.N. Lau, Science 317 (2007) 1530.
[23] M.A. Laakso, private communication (2007).
[24] A.H. Steinbach, J.M. Martinis, M.H. Devoret, Phys. Rev. Lett. 76 (1996) 3806.
[25] M. Henny, S. Oberholzer, C. Strunk, C. Schönenberger, Phys. Rev. B 59 (1999) 2871.
[26] K. Ziegler, Physica E 40 (2007) 2622.
[27] F. Wu, T. Tsuneta, R. Tarkiainen, D. Gunnarsson, T.-H. Wang, P.J. Hakonen, Phys. Rev. B 75 (2007) 125419.
[28] L. DiCarlo, J.R. Williams, Y. Zhang, D.T. McClure, C.M. Marcus, Phys. Rev. Lett. 100 (2008) 156801.
[29] C.H. Lewenkopf, E.R. Mucciolo, A.H. Castro Neto, Phys. Rev. B 77 (2008) 081410(R).
[30] M. Titov, Europhys. Lett. 79 (2007) 17004.
[31] A.F. Morpurgo, F. Guinea, Phys. Rev. Lett. 97 (2006) 196804.
[32] M.I. Katsnelson, K.S. Novoselov, A.K. Geim, Nature Phys. 2 (2006) 620.
[33] A. Rycerz, J. Tworzydło, C.W. Beenakker, Europhys. Lett. 79 (2007) 57003.
[34] P. San-Jose, E. Prada, D.S. Golubev, Phys. Rev. B 76 (2007) 195445.